

DynaMoN: Motion-Aware Fast and Robust Camera Localization for Dynamic Neural Radiance Fields

Nicolas Schischka^{1*}, Hannah Schieber^{2,3*}, Mert Asim Karaoglu^{1,4*}, Melih Gorgulu¹, Florian Grötzner¹, Alexander Ladikos⁴, Nassir Navab^{1,5}, Daniel Roth², and Benjamin Busam¹

Abstract—The accurate reconstruction of dynamic scenes with neural radiance fields is significantly dependent on the estimation of camera poses. Widely used structure-from-motion pipelines encounter difficulties in accurately tracking the camera trajectory when faced with separate dynamics of the scene content and the camera movement. To address this challenge, we propose **Dynamic Motion-Aware Fast and Robust Camera Localization for Dynamic Neural Radiance Fields (DynaMoN)**. DynaMoN utilizes semantic segmentation and generic motion masks to handle dynamic content for initial camera pose estimation and statics-focused ray sampling for fast and accurate novel-view synthesis. Our novel iterative learning scheme switches between training the NeRF and updating the pose parameters for an improved reconstruction and trajectory estimation quality. The proposed pipeline shows significant acceleration of the training process. We extensively evaluate our approach on two real-world dynamic datasets, the TUM RGB-D dataset and the BONN RGB-D Dynamic dataset. DynaMoN improves over the state-of-the-art both in terms of reconstruction quality and trajectory accuracy. We plan to make our code public to enhance research in this area. Code available: <https://hannahhaensen.github.io/DynaMoN/>.

Index Terms—Localization, Mapping

I. INTRODUCTION

ENABLING novel view synthesis (NVS) on dynamic scenes often requires multi-camera setups [1]. However, everyday dynamic scenes are often captured by one single moving camera, restricting the field of view [1]. To receive NVS or a 3D/4D scene representation, accurate camera poses are essential for such a representation. One way to retrieve camera poses is Simultaneous Localization and Mapping (SLAM). SLAM can result in multiple scene representations such as explicit voxel or surfel representations or neural radiance fields (NeRF) representations. The latter allows the

Manuscript received: August, 14, 2024; Revised October, 28, 2024; Accepted November, 21, 2024.

This paper was recommended for publication by Editor Javier Civera upon evaluation of the Associate Editor and Reviewers' comments. We thank d.hip for providing a campus stipend.

*equal contribution

¹Mert Asim Karaoglu, Benjamin Busam, Nassir Navab, Nicolas Schischka, Melih Gorgulu, Florian Grötzner are with Technical University of Munich, Munich, Germany mert.karaoglu@tum.de

²Daniel Roth and Hannah Schieber are with Human-Centered Computing and Extended Reality Lab, Technical University of Munich, School of Medicine and Health, Klinikum rechts der Isar, Orthopedics and Sports Orthopedics, Munich, Germany hannah.schieber@tum.de

³Hannah Schieber is with the Friedrich-Alexander Universität Erlangen-Nürnberg, Erlangen, Germany

⁴Mert Asim Karaoglu and Alexander Ladikos are with ImFusion GmbH, Munich, Germany

⁵Nassir Navab is with Johns Hopkins University, Baltimore, MD, USA
Digital Object Identifier (DOI): [10.1109/LRA.2024.3511399](https://doi.org/10.1109/LRA.2024.3511399).

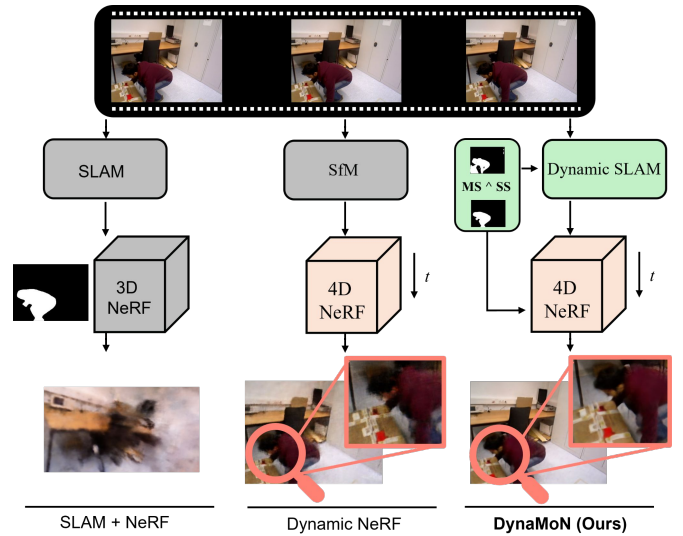


Fig. 1. NeRF combined with SLAM usually relies on static scenes (left). Approaches such as InstantNGP [3] can be used to mask out dynamic content [2], [11] (left) resulting still in reduced quality. Fully dynamic NeRF provides an implicit 4D (3D+time) representation; however, it relies on offline SfM, which can suffer in the presence of considerable motion (center). DynaMoN considers dynamics at all stages using motion segmentation (MS) and semantic segmentation (SS) (right). This enables a more robust camera tracking and NVS with a higher quality (ours, right).

rendering of photorealistic novel views from new, reasonable camera positions [2], [3]. While many are restricted to static scenes, dynamic NeRF [4], [5], [6], [7] allows NVS for dynamic scenes.

To enable NVS, accurate camera poses, usually retrieved via structure-from-motion (SfM) [8] or the Apple ARKit, are essential. SfM often demands hours of computation to estimate reasonable camera poses and is challenged by large-scale dynamic scenes. To overcome the limitation of time-intensive SfM, recent works combined SLAM and NeRF [9], [10], [11], [2]. SLAM provides faster results for the camera trajectory than classic SfM. However, by nature, scenes are more often dynamic than static. Existing Radiance Field-SLAM [9], [10], [11], [2], [12], [13] methods assume a static scene which poses difficulties when dynamic scene content is present as shown in Fig 1.

In this paper, we present DynaMoN, a motion-aware camera localization and visualization approach that can handle highly dynamic scenes.

- 1) We propose a novel combination of semantic segmentation and generic motion masks during our camera

localization to enable robust tracking of the camera path in a dynamic environment for dynamic neural radiance fields.

- 2) A statics-focused ray sampling building upon our dynamic masks is introduced to enhance our dynamic NeRF representation by refining the camera poses.

Overall, (1) and (2) improve the camera poses and in turn improve the NVS, leading to improved NVS quality in scenes with strong motions.

We conduct experiments on two challenging datasets, namely the dynamic subset of the TUM RGB-D [14] and the BONN RGB-D Dynamic [15] dataset. The considered masking in DynaMoN allows us to outperform existing approaches in terms of trajectory error and NVS results on these datasets.

II. RELATED WORK

DynaMoN combines dynamic NeRF with fast and robust motion-aware camera localization. Therefore, related work covers camera localization, camera localization for NVS, and neural representation for dynamic scenes.

A. Camera Localization and Scene Dynamics

Previous work on camera localization based on visual odometry (VO) [16], SfM [8] and SLAM [17], [18], [19], [20] extensively study architectures built for static scene assumptions. However, these methods show limited performance and often fail when they are encountered with the dynamic content commonly existent in real-world scenes.

In recent years, various classical and learning-based methods have been introduced to induce and handle the dynamic motion of the scene for robust camera pose estimation. With an assumption of prior knowledge of the objects that can independently move in the scene, DS-SLAM [21] builds upon ORB-SLAM2 [20] and integrates a semantic segmentation network to mask out motion-prone content along with a moving consistency check in the tracking process. Similarly, Dai et al. [22] extend ORB-SLAM2 [20] to handle the dynamic content with sparse point-level dynamic motion segmentation estimated by the correlation of their individual transformations across the temporal dimension. Ye et al. [23] utilize dense optical flow and leverage a learning-based approach to estimate and mask out the content that moves independently of the rigid camera motion. Building a VO pipeline for highly dynamic stereo surgical videos, Hayoz et al. [24] combine background segmentation with an end-to-end learning-based method to estimate the contribution of each pixel's motion for camera pose optimization that is structured in a differentiable training architecture.

We build DynaMoN based on the findings of the prior work and utilize both the semantic segmentation [21] of motion-prone objects and dense learning-based motion segmentation [23] to mask out dynamic content within a SLAM architecture [19] to estimate camera pose. Furthermore, we leverage this information with our introduced static-focused ray sampling method to further fine-tune the camera poses during neural reconstruction.

B. Camera Localization and Radiance Fields

Neural implicit methods gained popularity for scene representation. Mildenhall et al. [25] introduce NeRF employing a multi-layer perceptron (MLP) to represent a static 3D scene enabling NVS. NeRF requires precise camera poses during training, which are typically obtained through SfM pipelines like COLMAP [8] that can take long computation times for large sets of input images.

Proposing an alternative solution that can jointly optimize camera poses and scene representation, Sucar et al. [26] reformulate NeRF in a SLAM framework for ordered sets of image sequences. Zhu et al. [9] extend this by arranging multiple NeRFs in a hierarchical structure, improving the reconstruction capabilities. Following this, NICER-SLAM [10] introduces the usage of estimated depth images for more accurate geometric reconstruction. Others [2], [11] utilize hash-based InstantNGP [3] for its fast novel view rendering capabilities. NeRF-SLAM [2] adapts the Droid-SLAM [19] framework and Orbeez-SLAM [11] leverages ORB-SLAM [20].

More recent works [12], [27], [13] utilize an explicit scene representation for static scenes, namely Gaussian Splatting (GS) [28] combined with SLAM architectures for even faster convergence and novel view rendering.

Unlike the prior work, our proposed method does not carry static-scene assumptions. To this end, we utilize a two-step approach that efficiently estimates the camera poses using a dynamics-aware SLAM method and represents the scene in a dynamic NeRF architecture [4] that is extended to further refine the initially estimated camera poses.

C. Neural Representation of Dynamic Scenes

Our world is inherently dynamic which violates commonly used static scene assumptions and representations [9], [10], [26], [11], [2], [3], [29], [25]. To represent dynamics [30], [31], the use of grid structures is common [4], [5], [7]. HexPlane [4] utilizes a 4D space-time grid divided into six feature planes. The feature vector is a 4D point in space-time projected onto each feature plane. Similarly, Tensor4d [5] builds upon a 4D tensor field using time-aware volumes projected onto nine 2D planes. TiNeuVox [7] represents dynamic scenes using time-aware voxel features to enable faster training. [32], [33] propose the usage of GS with point cloud initializations for dynamic scene representations.

Optimizing camera poses and view synthesis can improve results in static scenes [34], [35], [36], [29]. Liu et al. [37] introduce such an optimization for a dynamic NeRF using a static and a dynamic part.

We, in contrast, split the problem into the differentiation of static and dynamic content. Already at the initial camera pose estimation this split is considered. The dynamic environment is then represented by an efficient dynamic, 4D NeRF [4] utilizing the camera poses estimated from the static scene components, and further refining these poses based on the static parts of the images.

III. METHOD

We utilize robust and fast camera localization and an implicit scene representation, a dynamic NeRF, to enable NVS on

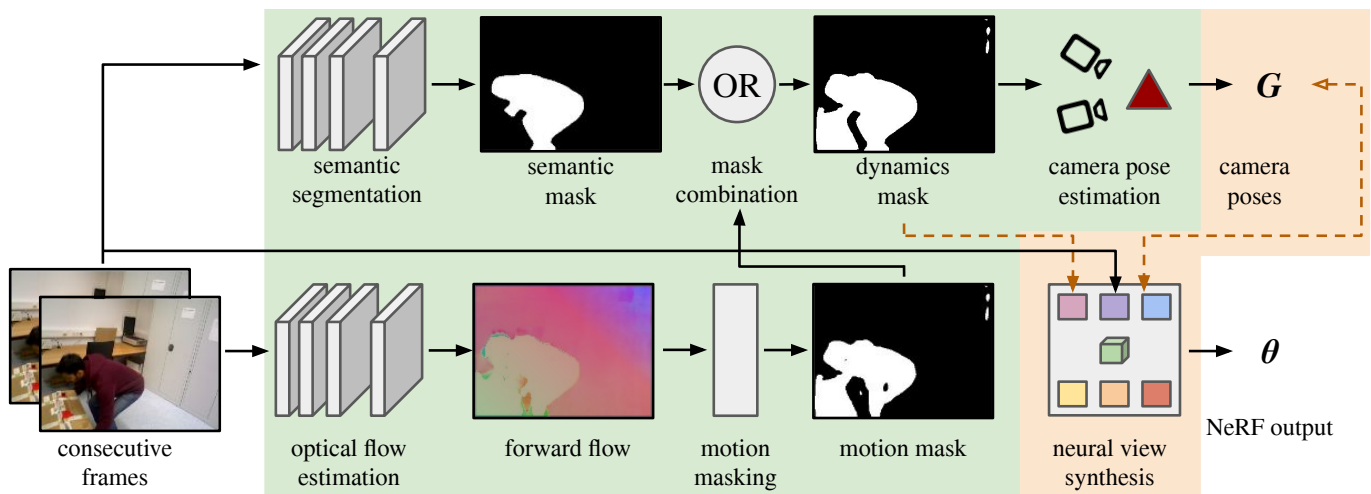


Fig. 2. DynaMoN retrieves consecutive RGB frames and applies semantic segmentation ($M_{SS} \rightarrow S_{S_i}$) and motion masks ($M_{MS} \rightarrow S_{M_i}$) on these input frames (I). Combining these masks (OR), we enable a motion-aware, fast and robust camera pose estimation G . Based on G , we produce a time-dependent output (Θ) using dynamic NeRF. During NeRF training, we utilize the previously computed masks to refine the camera poses (dashed lines). Dashed lines represent iterative updates on NeRF and pose parameters. We highlight our approach in green.

dynamic scenes. As input, we consider an RGB video captured in a dynamic environment using a single monocular moving camera without pose knowledge. This leads to two objectives: first, estimating the camera pose, and second, reconstructing the scene, which may comprise some deformation. We leverage masks to separate the scene dynamics from the static background for the former and utilize a 4D spatio-temporal neural representation for the latter. This allows to optimize for NVS while refining initial camera poses.

A. Robust Camera Localization in Dynamic Environments

NVS methods commonly employ rigid SfM, often COLMAP [8], for camera pose estimation which assumes a static scene. To cope with dynamics, it is possible to add binary masks to remove non-static regions. However, the high computation time of SfM approaches remains a drawback. In our approach, we target both robustness against dynamic scenes and a more efficient solution for pose estimation for dynamic moving cameras. Our underlying architecture is based on DROID-SLAM [19]. While it incorporates elements to cope with a certain level of scene dynamics, we found it can be improved by eliminating the contribution of the non-static regions for camera tracking. We do this by generating binary dynamics masks for each frame, which are combinations of semantic (M_{SS}) and motion masks (M_{MS}).

The semantic mask follows the paradigm that in real-world videos, the most prominent source of motion is often an object of known class. We, therefore, define $M_{SS} = \mathbb{1}(x > 0) \circ \sum_i M_{SS}(i)$ for all defined semantic classes $i \in S$ of the set S with the indicator function being 1 for positive values. Additional moving objects are covered through a motion mask M_{MS} . One example of a dynamic object outside of S is depicted by the moving box in Figure 2. Following DytanVO [38], our motion masks are generated using a CNN with the previous image, the forward optical flow and the estimated camera motion as input to iteratively refine the mask

along with updates of the relative motion between frames. Instead of random initialization, we begin with the motion mask of the previous frame to improve stability and lower the number of iterations in our refinement. We combine both masks as $M = \mathbb{1}(x > 0) (M_{SS} + M_{MS})$.

B. Neural Dynamic Scene Representation

To represent the dynamic scene, we build upon a state-of-the-art dynamic NeRF, HexPlane [4]. Targeting efficient optimization, fast rendering and high reconstruction quality, HexPlane [4] utilizes TensorRF [39] and constructs a 4D representation with three spatial and one temporal axes to create feature planes. Their pairwise combinations are then the input of a tiny MLP. The grid size of each axis is governed in a coarse-to-fine fashion along the training to improve convergence and naturally regularizes the local neighborhoods. For optimization, we follow the original NeRF ray casting and apply the pixel-wise photometric loss between the rendered RGB values C and the ground truth values \hat{C} , supported by a total variation regularization as:

$$\mathcal{L} = \frac{1}{|\mathcal{R}|} \sum_{\mathbf{r} \in \mathcal{R}} \|C(\mathbf{r}) - \hat{C}(\mathbf{r})\|_2^2 + \lambda_{TV} \mathcal{L}_{TV}. \quad (1)$$

While \mathcal{R} represents the sampled rays, \mathcal{L}_{TV} and λ_{TV} depict the total variation regularization and its weight.

C. Pose Refinement and Training Strategy

We utilize eqn. (1) as the objective function for training both the NeRF and refining the camera poses. During optimization, we employ an alternating training strategy in which every 5000 iterations, the parameters to be optimized are switched between the radiance field and the pose parameters. To improve the accuracy and robustness of the optimization, during the pose refinement phase, we constrain the sampled rays, \mathcal{R} , contributing to the loss to be elements of the static regions designated by the inverse dynamics masks. Furthermore, we

TABLE I

PERCENTAGE OF ORIENTATIONS FOR WHICH THE MEDIAN RRA IS BELOW THE SPECIFIED THRESHOLD [%] ON THE TUM RGB-D DATASET AND THE BONN RGB-D DYNAMIC DATASET.

Dataset	Metric	DROID-SLAM	OURS (MS&SS)	OURS (SS)	OURS (MS)
TUM RGB-D	median RRA@5 \uparrow	100.0	100.0	100.0	100.0
	median RRA@15 \uparrow	100.0	100.0	100.0	100.0
Bonn RGB-D	median RRA@5 \uparrow	61.05	61.89	61.86	61.88
	median RRA@15 \uparrow	91.29	91.45	91.46	91.27

also use the same masks to ensure that the total variation regularization is imposed only on the static components. As the amount of non-dynamic sampled rays can vary from image to image, we scale the learning rate η_s by the fraction of static pixels in the image to keep the optimization steps in the same magnitude:

$$\eta = \eta_s * \frac{n_{static}}{n_{static} + n_{dynamic}}, \quad (2)$$

where n_{static} and $n_{dynamic}$ represent the number of static and dynamic pixels in the image and η is the learning rate used for the pose refinement.

IV. EVALUATION

To evaluate our approach, we consider the translational absolute trajectory error (ATE) [40] using root mean square error (RMSE) in meters. To reason about the orientation, we employ the Relative Rotation Accuracy (RRA) as defined in [41] after synchronizing the poses to the GT to be invariant against the alignment of coordinate frames. We calculate the median RRA over all sequences and report the percentage of poses for which the RRA lies below a specified threshold. For NVS quality, we analyze the rendering quality of the novel dynamic views by reporting PSNR and SSIM [42].

A. Datasets

To assess DynaMoN, we evaluate both the camera localization and the NVS part with state-of-the-art approaches on two dynamic datasets. In total, we evaluate our approach on 33 dynamic sequences (9 from TUM-RGB-D, and 24 from BONN RGB-D). For NVS, we follow the usual splitting using every eighth frame for testing.

a) **TUM RGB-D - Dynamic subset [14]:** We used the nine dynamic sequences, with five sequences rated *slightly dynamic* and four *highly dynamic*. The images of the TUM RGB-D dataset have a resolution of 640×480 .

b) **BONN RGB-D Dynamic [15]:** The BONN RGB-D Dynamic dataset consists of 24 dynamic sequences and two static sequences with an image resolution of 640×480 .

B. Implementation Details

We implemented our approach in Python using PyTorch and evaluated it on one single workstation (Intel i9-10980XE CPU, NVIDIA GeForce RTX 3090 GPU 24GB, and 128GB RAM) unless otherwise specified.

For semantic masking, we use DeepLabV3 [48]/ResNet50 [49] trained on COCO [50] to obtain human masks. For motion masking, we apply DytanVO [38]. In practice, initialized with the motion mask of the previous frame, we found that setting

the number of iterations for motion mask refinement to two provides stable convergence.

When the camera motion exceeds that of the DytanVO training sequences, the motion segmentation module produces more false positives. To counter this, we set a threshold of 60% for the maximum number of motion pixels; masks exceeding this threshold are discarded to maintain sufficient pixels for dense bundle adjustment. Additionally, a pixel is considered dynamic only if the confidence is above 0.95 for the first mask refinement step and 0.98 for subsequent steps.

For NVS, we use the full image size. During camera localization, the images are downsampled by half to remain consistent with existing trajectory experiments [19].

We set the loss parameter λ_{TV} to 0.005 and sample $|\mathcal{R}| = 1,024$ rays per batch. We use the default optimization settings for the dynamic NeRF [4], with a multi-step learning rate decay scheduler for pose refinement. The initial learning rate is 1×10^{-5} , decayed by a factor of 0.9 every 1,000 iterations and reset in each pose optimization cycle. The learning rate is scaled by the percentage of static pixels in the image. The number of optimization iterations is set to 200,000, unless specified otherwise.

C. Camera Localization Quality

Our results on all datasets show a lower translational trajectory error compared to state-of-the-art approaches, see Table II and Table III. We compare RGB-D-based and monocular SLAM approaches with our proposed camera retrieval method using only motion masks (MS), using only semantic masks (SS) as well as using both types of masks in combination (MS&SS). Looking at the mean value of the RMSE of the translational ATE over all sequences, our approach performs similarly to DROID-SLAM on TUM RGB-D. However, the maximum error value is much lower, which shows that it is less prone to failure when applied to real-world scenarios. On the BONN RGB-D Dynamic dataset, our approach outperforms the state-of-the-art approaches in terms of mean and maximum trajectory error for translation. Moreover, comparing the RRA, see Table I, our MS&SS-model achieves higher values than DROID-SLAM on the BONN RGB-D dataset, while all methods perform equally well on TUM RGB-D. It can be noted that using one type of mask is usually sufficient to improve over DROID-SLAM. In some cases, like the person-tracking scene, where the combination performs worse than SS or MS, the SLAM backbone seems to have too less pixels left for the bundle adjustment.

D. Novel View Synthesis Quality

To evaluate the NVS quality of our approach, we consider several aspects. First, we compare it with the traditional way of generating camera ground truth for 4D NeRF [4] and 4D GS [32] using COLMAP, see Tables IV and V. We follow the implementation of InstantNGP [3] to retrieve the COLMAP ground truth. Second, we compare our approach with RoDynRF [37] without initial COLMAP poses, shown in Table IV. We follow RoDynRF's training guidelines. Third, we highlight the influence of the iterative pose refinement

TABLE II

RMSE OF THE TRANSLATIONAL ATE [M] ON TUM RGB-D [14]. THE UPPER ROWS ARE THE SLIGHTLY DYNAMIC SCENES AND THE LOWER ROWS ARE THE HIGHLY DYNAMIC SCENES. THE - DENOTES THAT NO RESULTS WERE REPORTED FOR THESE SEQUENCES.

Sequences	RGB-D					RGB					
	DVO-SLAM [44]	ORB-SLAM2 [20]	PointCorr [22]	DynaPix-D [43]	Yu et al. [45]	DytanVO [38]	DeFlowSLAM [23]	DROID-SLAM [19]	OURS (MS&SS)	OURS (SS)	OURS (MS)
fr2/desk-person	0.104	0.006	0.008	-	-	1.166	0.013	0.006	0.007	0.007	0.006
fr3/sitting-static	0.012	0.008	0.010	-	0.006	0.016	0.007	0.005	0.005	0.005	0.005
fr3/sitting-xyz	0.242	0.010	0.009	-	-	0.260	0.015	0.009	0.010	0.010	0.009
fr3/sitting-rpy	0.176	0.025	0.023	-	-	0.046	0.027	0.022	0.024	0.024	0.021
fr3/sitting-halfsphere	0.220	0.025	0.024	-	0.018	0.310	0.025	0.014	0.023	0.028	0.019
fr3/walking-static	0.752	0.408	0.011	0.007	0.009	0.021	0.007	0.012	0.007	0.007	0.014
fr3/walking-xyz	1.383	0.722	0.087	0.014	0.014	0.028	0.018	0.016	0.014	0.014	0.014
fr3/walking-rpy	1.292	0.805	0.161	0.123	0.031	0.155	0.057	0.040	0.031	0.036	0.039
fr3/walking-halfsphere	1.014	0.723	0.035	0.023	0.020	0.385	0.420	0.022	0.019	0.019	0.020
Mean/Max	0.577/1.383	0.304/0.805	0.041/0.161	-	-	0.265/1.166	0.065/0.420	0.016/0.040	0.016/0.031	0.017/0.036	0.016/0.039

TABLE III

RMSE OF THE TRANSLATIONAL ATE [M] ON BONN RGB-D DYNAMIC [15]. RGB-D RESULTS ARE REPORTED BY PALAZZOLO ET AL. [15]. FOR DROID-SLAM AND OURS, WE CALCULATED THE RESULTS.

Sequences	RGB-D				RGB			
	ReFusion [15]	StaticFusion [46]	DynaSLAM (G) [47]	DynaSLAM (N+G) [47]	DROID-SLAM [19]	OURS (MS&SS)	OURS (SS)	OURS (MS)
balloon	0.175	0.233	0.050	0.030	0.075	0.028	0.030	0.068
balloon2	0.254	0.293	0.142	0.029	0.041	0.027	0.027	0.038
balloon_tracking	0.302	0.221	0.156	0.049	0.035	0.034	0.037	0.036
balloon_tracking2	0.322	0.366	0.192	0.035	0.026	0.032	0.029	0.028
crowd	0.204	3.586	1.065	0.016	0.052	0.035	0.033	0.061
crowd2	0.155	0.215	1.217	0.031	0.065	0.028	0.029	0.056
crowd3	0.137	0.168	0.835	0.038	0.046	0.032	0.052	0.055
kidnapping_box	0.148	0.336	0.026	0.029	0.020	0.021	0.020	0.020
kidnapping_box2	0.161	0.263	0.033	0.035	0.017	0.017	0.017	0.017
moving_no_box	0.071	0.141	0.317	0.232	0.023	0.013	0.014	0.014
moving_no_box2	0.179	0.364	0.052	0.039	0.040	0.027	0.027	0.026
moving_o_box	0.343	0.331	0.544	0.044	0.177	0.152	0.152	0.167
moving_o_box2	0.528	0.309	0.589	0.263	0.236	0.175	0.176	0.176
person_tracking	0.289	0.484	0.714	0.061	0.043	0.148	0.033	0.024
person_tracking2	0.463	0.626	0.817	0.078	0.054	0.022	0.023	0.035
placing_no_box	0.106	0.125	0.645	0.575	0.078	0.021	0.042	0.018
placing_no_box2	0.141	0.177	0.027	0.021	0.030	0.020	0.019	0.020
placing_no_box3	0.174	0.256	0.327	0.058	0.025	0.022	0.022	0.022
placing_o_box	0.571	0.330	0.267	0.255	0.127	0.172	0.173	0.117
removing_no_box	0.041	0.136	0.016	0.016	0.016	0.015	0.015	0.015
removing_no_box2	0.111	0.129	0.022	0.021	0.020	0.019	0.020	0.021
removing_o_box	0.222	0.334	0.362	0.291	0.189	0.177	0.179	0.181
synchronous	0.441	0.446	0.977	0.015	0.006	0.007	0.007	0.006
synchronous2	0.022	0.027	0.887	0.009	0.012	0.006	0.007	0.011
Mean/Max	0.232/0.571	0.412/3.586	0.428/1.217	0.095/0.575	0.061/0.236	0.052/ 0.177	0.049/0.179	0.051/0.181

by training both DynaMoN and HexPlane with our initially localized poses, see Tables IV, Table V and VI. Qualitative examples of renderings on both datasets can be found in Figure 3.

On both datasets, COLMAP is challenged by the dynamics, and training with COLMAP camera poses can only be performed on a subset of scenes. DynaMoN retrieves all camera poses for both datasets, see Tables II and III. As visualized in Figure 3, the visual results of COLMAP-based NeRF are noisy on both datasets. DynaMoN’s camera poses can show improved results. The complete DynaMoN can further improve details. In terms of PSNR/SSIM, DynaMoN leads to a higher NVS quality compared to HexPlane without refined poses, RoDynRF, and when using COLMAP for the camera poses for either 4D NeRF or 4D GS, see Table IV.

E. Robustness on Sparse Trajectories

Dynamic scenes pose more challenges regarding the robustness of an approach compared to static environments. In

Table VI, we showcase the robustness of our approach. We use only every tenth frame of the crowd2 sequence from the BONN RGB-D Dynamic dataset. As reported in Table VI, we show how the underlying camera localization approach influences the NVS result. When comparing DROID-SLAM camera poses to the ones from our DynaMoN backbone and our neural camera pose refinement, the best NVS result can be achieved using DynaMoN. Looking at the PSNR values in Table VI, it can be noted that each of our proposed components increases the reconstruction quality. Thus, when confronted with a sparse trajectory of a highly dynamic scene, DynaMoN outperforms pure DROID-SLAM making it more robust to realistic, real-world scenarios with imperfect camera recordings.

F. Runtime and Memory Evaluation

We compare the runtime and memory consumption of DynaMoN with RoDynRF [37] on a workstation with an

TABLE IV

NVS RESULTS ON TUM RGB-D. THE UPPER ROWS ARE THE SLIGHTLY DYNAMIC SCENES AND THE LOWER ROWS ARE THE HIGHLY DYNAMIC SCENES. THE - DENOTES THAT THE CAMERA POSE COULD NOT BE REGRESSED. THE * DENOTES RANDOM POINT CLOUD INITIALIZATION, AS THE ONE FROM COLMAP LEAD TO NO CONVERGENCE. WE REPORT PSNR/SSIM.

PSNR \uparrow /SSIM \uparrow	RGB-D		RGB		
	RoDynRF [37]	4D Gaussians [32] (COLMAP)	HexPlane [4] (COLMAP)	HexPlane + DynaMoN Backbone (Ours)	DynaMoN (Ours)
Sequences					
fr2/desk-person	6.05 / 0.127	-	-	23.04 / 0.680	24.83 / 0.725
fr3/sitting-static	9.67 / 0.123	-	-	28.55 / 0.899	28.95 / 0.903
fr3/sitting-xyz	10.10 / 0.150	26.40 / 0.886	19.98 / 0.589	25.90 / 0.848	26.15 / 0.850
fr3/sitting-rpy	8.35 / 0.121	24.15 / 0.814	16.63 / 0.472	25.76 / 0.843	26.40 / 0.853
fr3/sitting-halfsphere	7.46 / 0.157	24.42 / 0.830	24.25 / 0.793	24.05 / 0.792	24.60 / 0.799
fr3/walking-static	10.01 / 0.159	16.39 / 0.575*	20.27 / 0.650	25.84 / 0.849	26.25 / 0.853
fr3/walking-xyz	10.02 / 0.171	-	-	24.05 / 0.797	24.34 / 0.796
fr3/walking-rpy	8.81 / 0.201	-	-	24.18 / 0.790	24.70 / 0.796
fr3/walking-halfsphere	8.79 / 0.205	21.72 / 0.746	22.01 / 0.692	24.05 / 0.781	24.27 / 0.779
Mean	8.84 / 0.157	-	-	25.05 / 0.809	25.60 / 0.819

TABLE V

NVS RESULTS ON BONN RGB-D DYNAMIC. THE - DENOTES THAT THE CAMERA POSE COULD NOT BE REGRESSED. WE REPORT PSNR/SSIM.

PSNR \uparrow /SSIM \uparrow	RGB		
	HexPlane (COLMAP)	HexPlane + DynaMoN Backbone (Ours)	DynaMoN (Ours)
Sequences			
balloon	-	29.83 / 0.868	29.84 / 0.866
balloon2	-	27.61 / 0.841	28.31 / 0.847
balloon_tracking	-	29.27 / 0.847	29.55 / 0.846
balloon_tracking2	-	29.68 / 0.860	30.56 / 0.862
crowd	-	27.92 / 0.831	28.40 / 0.829
crowd2	-	26.68 / 0.825	27.97 / 0.827
crowd3	-	26.57 / 0.815	27.40 / 0.827
kidnapping_box	-	30.43 / 0.870	30.59 / 0.869
kidnapping_box2	-	30.28 / 0.860	30.18 / 0.857
moving_no_box	30.67 / 0.881	30.32 / 0.866	30.36 / 0.862
moving_no_box2	31.14 / 0.890	30.57 / 0.874	30.62 / 0.870
moving_o_box	29.21 / 0.889	30.26 / 0.884	31.08 / 0.888
moving_o_box2	-	29.82 / 0.875	29.40 / 0.875
person_tracking	26.57 / 0.808	27.78 / 0.843	28.71 / 0.845
person_tracking2	-	27.47 / 0.837	27.80 / 0.833
placing_no_box	25.73 / 0.780	30.94 / 0.869	31.23 / 0.870
placing_no_box2	-	31.18 / 0.885	31.45 / 0.884
placing_no_box3	-	30.79 / 0.879	30.83 / 0.875
placing_o_box	-	30.42 / 0.886	31.12 / 0.890
removing_no_box	-	30.66 / 0.879	30.85 / 0.877
removing_no_box2	31.13 / 0.887	30.73 / 0.871	30.86 / 0.870
removing_o_box	31.13 / 0.887	30.30 / 0.880	30.76 / 0.882
synchronous	-	28.42 / 0.835	28.93 / 0.834
synchronous2	-	28.85 / 0.887	30.18 / 0.891
Mean	-	29.45 / 0.861	29.87 / 0.861

TABLE VI

ANALYSIS OF DIFFERENT POSE RETRIEVAL STEPS ON NVS QUALITY, EVALUATED ON THE CROWD2 SCENE OF THE BONN RGB-D DYNAMIC DATASET. WE ASSESS ROBUSTNESS USING A SPARSE INPUT TRAJECTORY (EVERY 10TH FRAME).

Approach	PSNR \uparrow /SSIM \uparrow
DROID-SLAM [19] + HexPlane [4]	16.46 / 0.661
Our initial poses + HexPlane [4]	17.07 / 0.660
DynaMoN (Ours)	17.31 / 0.659

NVIDIA RTX 4090 graphics card with 24 GB of VRAM. We report the results for the TUM RGB-D fr2/desk-person sequence in Table VII as it is by far the longest scene of both datasets comprising 4067 frames. Using the COLMAP configuration from Instant-NGP, COLMAP runs for 38:28:16

TABLE VII

ANALYSIS OF THE RUNTIME ON TUM RGB-D FR2/DESK-PERSON. OURS REFERS TO 200,000 ITERATIONS / 1,024 BATCH SIZE. THE SYMBOL \ddagger INDICATES 100,000 ITERATIONS / 512 BATCH SIZE, WHILE \dagger REPRESENTS 100,000 ITERATIONS / 1.024 BATCH SIZE. TIME IS GIVEN IN THE FORMAT HOURS:MINUTES:SECONDS

Approach	Pre-processing \downarrow	Training \downarrow	Rendering \downarrow	Total \downarrow	PSNR \uparrow /SSIM \uparrow
COLMAP [8]	38:28:16	-	-	-	-
RoDynRF [37] \ddagger	01:52:55	08:00:44	00:11:15	10:04:54	6.05 / 0.127
Ours	00:13:49	09:49:25	00:42:32	10:45:46	24.83 / 0.725
Ours \dagger	00:14:12	05:04:19	00:42:20	06:00:51	23.95 / 0.702
Ours \ddagger	00:13:41	04:43:23	01:03:21	06:00:25	23.43 / 0.690

(hours:minutes:seconds), see Table VII. In terms of memory requirement, RoDynRF can only be trained with a batch size of 512 in this setting, while DynaMoN is more memory-efficient, enabling a batch size of 1024. From the experiments, it can be concluded that the total time for pre-processing, training and rendering of DynaMoN is comparable to RoDynRF if the default training strategy with 200000 iterations is utilized. However, if our model is trained for 100000 iterations which is the default value of RoDynRF, the total time can be greatly reduced without a significant drop in photometric accuracy. For this shorter training, the NeRF and pose optimization of DynaMoN alternate every 2500 iterations. Furthermore, a decrease of the batch size to the same value as in the competitor method, RoDynRF, further speeds up the training time at the cost of a longer rendering time while staying comparably accurate.

It has to be noted that the pre-processing of RoDynRF consisting of monocular depth prediction, optical flow prediction, motion mask generation and data loading takes about eight times longer than our pre-processing loading the data and generating initial poses as well as motion masks.

V. DISCUSSION

In comparison to traditional sparse reconstructions [18], [17], [19], our approach addresses camera localization and dynamic NVS in combination. While this leads to more pleasing 3D visualizations and NVS results, the computing time is higher compared to traditional camera localization and non-dynamic 3D representation methods [9], [10], [11]. Nevertheless, compared to combined dynamic camera localization



Fig. 3. Qualitative Results for NVS on TUM RGB-D (top) and BONN RGB-D Dynamic (bottom). Ground Truth (left), novel views views from HexPlane + COLMAP (2nd column), improved camera poses from our backbone (3rd column), and our full model (right).

and dynamic NVS approaches [37], our approach requires only 60% of the training time when using the same number of iterations and batch size, while being more robust in more dynamic scenes with dynamic camera motion.

Moreover, our approach shows an improved performance compared to the state-of-the-art for camera localization. Only using our motion masks already improves the performance. Moreover, for scenes with large motions, the combination with semantic segmentation masks provides significantly improved camera localization results. The results presented in Table IV indicate that RoDynRF [37], despite being a state-of-the-art method that integrates combined camera regression with NVS, faces significant challenges in handling highly dynamic camera movements and dynamic scenes. In contrast, our method demonstrates superior robustness and yields improved outcomes when compared to both RoDynRF [37] and HexPlane [4] employing COLMAP poses on the BONN RGB-D Dynamic and TUM RGB-D dataset. Furthermore, our iterative pose refinement process enhances robustness, as evidenced in Table VI, and achieves better performance in NVS on both datasets.

Looking at the results of 4D GS with COLMAP poses, combining robust camera localization and 4D GS seems to be a promising future research direction.

VI. LIMITATIONS

DynaMoN is constrained by the scene representation capabilities of dynamic NeRFs. Although it performs well on large-scale datasets with up to over 4,000 images, handling scenes with close to 8,000 frames introduces significant challenges to the camera pose localization [51] and the NeRF [52]. Nevertheless, our method works effectively with datasets like TUM RGB-D and BONN RGB-D Dynamic. Still, larger datasets [53] pose challenges, for NeRF and the camera localization [51]. The underlying dynamic NeRF in this work has difficulties representing environments of this scale, limiting its applicability to more extensive datasets.

VII. CONCLUSION

We present DynaMoN, a motion-aware, fast and robust camera localization approach for NVS. DynaMoN can cope with the motion of objects of known and unknown classes using the combined segmentation and motion mask resulting in the dynamics mask. DynaMoN retrieves camera poses

faster and is more robust to scene dynamics in comparison to traditional SfM approaches, enabling a more accurate 4D scene representation. In addition, DynaMoN is trained with a novel iterative training scheme that refines NeRF parameters and the initially provided poses in an alternating fashion. Compared to the state-of-the-art, DynaMoN outperforms other dynamic camera localization approaches and shows better results for NVS on scenes with high camera motion.

REFERENCES

- [1] M. Broxton, J. Flynn, R. Overbeck, D. Erickson, P. Hedman, M. Duvall, J. Dourgarian, J. Busch, M. Whalen, and P. Debevec, "Immersive light field video with a layered mesh representation," *ACM Trans. Graph.*, vol. 39, no. 4, aug 2020.
- [2] A. Rosinol, J. J. Leonard, and L. Carlone, "Nerf-slam: Real-time dense monocular slam with neural radiance fields," in *2023 IEEE/RSJ International Conference on Intelligent Robots and Systems (IROS)*. IEEE, 2023, pp. 3437–3444.
- [3] T. Müller, A. Evans, C. Schied, and A. Keller, "Instant neural graphics primitives with a multiresolution hash encoding," *ACM Transactions on Graphics (ToG)*, vol. 41, no. 4, pp. 1–15, 2022.
- [4] A. Cao and J. Johnson, "Hexplane: A fast representation for dynamic scenes," in *Proceedings of the IEEE/CVF Conference on Computer Vision and Pattern Recognition*, 2023, pp. 130–141.
- [5] R. Shao, Z. Zheng, H. Tu, B. Liu, H. Zhang, and Y. Liu, "Tensor4d: Efficient neural 4d decomposition for high-fidelity dynamic reconstruction and rendering," in *Proceedings of the IEEE/CVF Conference on Computer Vision and Pattern Recognition*, 2023, pp. 16 632–16 642.
- [6] L. Song, A. Chen, Z. Li, Z. Chen, L. Chen, J. Yuan, Y. Xu, and A. Geiger, "Nerfplayer: A streamable dynamic scene representation with decomposed neural radiance fields," *IEEE Transactions on Visualization and Computer Graphics*, pp. 2732–2742, 2023.
- [7] J. Fang, T. Yi, X. Wang, L. Xie, X. Zhang, W. Liu, M. Nießner, and Q. Tian, "Fast dynamic radiance fields with time-aware neural voxels," in *SIGGRAPH Asia 2022 Conference Papers*, 2022.
- [8] J. L. Schonberger and J.-M. Frahm, "Structure-from-motion revisited," in *Proceedings of the IEEE conference on computer vision and pattern recognition*, 2016, pp. 4104–4113.
- [9] Z. Zhu, S. Peng, V. Larsson, W. Xu, H. Bao, Z. Cui, M. R. Oswald, and M. Pollefeys, "Nice-slam: Neural implicit scalable encoding for slam," in *Proceedings of the IEEE/CVF Conference on Computer Vision and Pattern Recognition*, 2022, pp. 12 786–12 796.
- [10] Z. Zhu, S. Peng, V. Larsson, Z. Cui, M. R. Oswald, A. Geiger, and M. Pollefeys, "Nicer-slam: Neural implicit scene encoding for rgb slam," in *2024 International Conference on 3D Vision (3DV)*. IEEE, 2024, pp. 42–52.
- [11] C.-M. Chung, Y.-C. Tseng, Y.-C. Hsu, X.-Q. Shi, Y.-H. Hua, J.-F. Yeh, W.-C. Chen, Y.-T. Chen, and W. H. Hsu, "Orbeez-slam: A real-time monocular visual slam with orb features and nerf-realized mapping," in *2023 IEEE International Conference on Robotics and Automation (ICRA)*. IEEE, 2023, pp. 9400–9406.
- [12] H. Matsuki, R. Murai, P. H. Kelly, and A. J. Davison, "Gaussian splatting slam," in *Proceedings of the IEEE/CVF Conference on Computer Vision and Pattern Recognition (CVPR)*, June 2024, pp. 18 039–18 048.

- [13] S. Zhu, R. Qin, G. Wang, J. Liu, and H. Wang, "Semgauss-slam: Dense semantic gaussian splatting slam," 2024. [Online]. Available: <https://arxiv.org/abs/2403.07494>
- [14] J. Sturm, N. Engelhard, F. Endres, W. Burgard, and D. Cremers, "A benchmark for the evaluation of rgb-d slam systems," in *Proc. of the International Conference on Intelligent Robot Systems (IROS)*, 2012.
- [15] E. Palazzolo, J. Behley, P. Lottes, P. Giguère, and C. Stachniss, "ReFusion: 3D Reconstruction in Dynamic Environments for RGB-D Cameras Exploiting Residuals," in *2019 IEEE/RSJ International Conference on Intelligent Robots and Systems (IROS)*. IEEE, 2019, pp. 7855–7862.
- [16] J. Engel, V. Koltun, and D. Cremers, "Direct sparse odometry," *IEEE transactions on pattern analysis and machine intelligence*, vol. 40, no. 3, pp. 611–625, 2017.
- [17] R. Mur-Artal, J. M. M. Montiel, and J. D. Tardos, "Orb-slam: a versatile and accurate monocular slam system," *IEEE transactions on robotics*, vol. 31, no. 5, pp. 1147–1163, 2015.
- [18] C. Campos, R. Elvira, J. J. G. Rodríguez, J. M. Montiel, and J. D. Tardós, "Orb-slam3: An accurate open-source library for visual, visual-inertial, and multimap slam," *IEEE Transactions on Robotics*, vol. 37, no. 6, pp. 1874–1890, 2021.
- [19] Z. Teed and J. Deng, "Droid-slam: Deep visual slam for monocular, stereo, and rgb-d cameras," *Advances in neural information processing systems*, vol. 34, pp. 16558–16569, 2021.
- [20] R. Mur-Artal and J. D. Tardós, "Orb-slam2: An open-source slam system for monocular, stereo, and rgb-d cameras," *IEEE transactions on robotics*, vol. 33, no. 5, pp. 1255–1262, 2017.
- [21] C. Yu, Z. Liu, X.-J. Liu, F. Xie, Y. Yang, Q. Wei, and Q. Fei, "Dslam: A semantic visual slam towards dynamic environments," in *2018 IEEE/RSJ international conference on intelligent robots and systems (IROS)*. IEEE, 2018, pp. 1168–1174.
- [22] W. Dai, Y. Zhang, P. Li, Z. Fang, and S. Scherer, "Rbg-d slam in dynamic environments using point correlations," *IEEE Transactions on Pattern Analysis and Machine Intelligence*, vol. 44, no. 1, pp. 373–389, 2020.
- [23] W. Ye, X. Yu, X. Lan, Y. Ming, J. Li, H. Bao, Z. Cui, and G. Zhang, "Deflowslam: Self-supervised scene motion decomposition for dynamic dense slam," *arXiv preprint arXiv:2207.08794*, 2022.
- [24] M. Hayoz, C. Hahne, M. Gallardo, D. Candinas, T. Kurmann, M. Allan, and R. Schnitman, "Learning how to robustly estimate camera pose in endoscopic videos," *International journal of computer assisted radiology and surgery*, vol. 18, no. 7, pp. 1185–1192, 2023.
- [25] B. Mildenhall, P. P. Srinivasan, M. Tancik, J. T. Barron, R. Ramamoorthi, and R. Ng, "Nerf: Representing Scenes as Neural Radiance Fields for View Synthesis," in *European Conference on Computer Vision*. Springer, 2020, pp. 405–421.
- [26] E. Sucar, S. Liu, J. Ortiz, and A. J. Davison, "imap: Implicit mapping and positioning in real-time," in *Proceedings of the IEEE/CVF International Conference on Computer Vision*, 2021, pp. 6229–6238.
- [27] C. Yan, D. Qu, D. Xu, B. Zhao, Z. Wang, D. Wang, and X. Li, "Gslam: Dense visual slam with 3d gaussian splatting," in *Proceedings of the IEEE/CVF Conference on Computer Vision and Pattern Recognition*, 2024, pp. 19595–19604.
- [28] B. Kerbl, G. Kopanas, T. Leimkühler, and G. Drettakis, "3d gaussian splatting for real-time radiance field rendering," *ACM Trans. Graph.*, vol. 42, no. 4, pp. 139–1, 2023.
- [29] H. Schieber, F. Deuser, B. Egger, N. Oswald, and D. Roth, "Nerfrtrinsic four: An end-to-end trainable nerf jointly optimizing diverse intrinsic and extrinsic camera parameters," *Computer Vision and Image Understanding*, vol. 249, p. 104206, 2024.
- [30] A. Pumarola, E. Corona, G. Pons-Moll, and F. Moreno-Noguer, "D-nerf: Neural radiance fields for dynamic scenes," in *Proceedings of the IEEE/CVF Conference on Computer Vision and Pattern Recognition*, 2021, pp. 10318–10327.
- [31] K. Park, U. Sinha, J. T. Barron, S. Bouaziz, D. B. Goldman, S. M. Seitz, and R. Martin-Brualla, "Nerfies: Deformable neural radiance fields," in *Proceedings of the IEEE/CVF International Conference on Computer Vision*, 2021, pp. 5865–5874.
- [32] G. Wu, T. Yi, J. Fang, L. Xie, X. Zhang, W. Wei, W. Liu, Q. Tian, and X. Wang, "4d gaussian splatting for real-time dynamic scene rendering," in *Proceedings of the IEEE/CVF Conference on Computer Vision and Pattern Recognition (CVPR)*, June 2024, pp. 20310–20320.
- [33] J. Luiten, G. Kopanas, B. Leibe, and D. Ramanan, "Dynamic 3d gaussians: Tracking by persistent dynamic view synthesis," in *2024 International Conference on 3D Vision (3DV)*. IEEE, 2024, pp. 800–809.
- [34] Z. Wang, S. Wu, W. Xie, M. Chen, and V. A. Prisacariu, "NeRF-: Neural radiance fields without known camera parameters," *arXiv preprint arXiv:2102.07064*, 2021.
- [35] Q. Meng, A. Chen, H. Luo, M. Wu, H. Su, L. Xu, X. He, and J. Yu, "GNerF: GAN-Based Neural Radiance Field Without Posed Camera," in *Proceedings of the IEEE/CVF International Conference on Computer Vision (ICCV)*, Oct. 2021, pp. 6351–6361.
- [36] L. Yen-Chen, P. Florence, J. T. Barron, A. Rodriguez, P. Isola, and T.-Y. Lin, "iNeRF: Inverting Neural Radiance Fields for Pose Estimation," in *2021 IEEE/RSJ International Conference on Intelligent Robots and Systems (IROS)*, 2021, pp. 1323–1330.
- [37] Y.-L. Liu, C. Gao, A. Meuleman, H.-Y. Tseng, A. Saraf, C. Kim, Y.-Y. Chuang, J. Kopf, and J.-B. Huang, "Robust dynamic radiance fields," in *Proceedings of the IEEE/CVF Conference on Computer Vision and Pattern Recognition*, 2023, pp. 13–23.
- [38] S. Shen, Y. Cai, W. Wang, and S. Scherer, "Dytanvo: Joint refinement of visual odometry and motion segmentation in dynamic environments," in *2023 IEEE International Conference on Robotics and Automation (ICRA)*. IEEE, 2023, pp. 4048–4055.
- [39] A. Chen, Z. Xu, A. Geiger, J. Yu, and H. Su, "Tensorf: Tensorial radiance fields," in *European Conference on Computer Vision*. Springer, 2022, pp. 333–350.
- [40] Z. Zhang and D. Scaramuzza, "A tutorial on quantitative trajectory evaluation for visual (-inertial) odometry," in *2018 IEEE/RSJ International Conference on Intelligent Robots and Systems (IROS)*. IEEE, 2018, pp. 7244–7251.
- [41] J. Wang, C. Rupprecht, and D. Novotny, "Posediffusion: Solving pose estimation via diffusion-aided bundle adjustment," in *Proceedings of the IEEE/CVF International Conference on Computer Vision*, 2023, pp. 9773–9783.
- [42] Z. Wang, A. C. Bovik, H. R. Sheikh, and E. P. Simoncelli, "Image quality assessment: from error visibility to structural similarity," *IEEE transactions on image processing*, vol. 13, no. 4, pp. 600–612, 2004, publisher: IEEE.
- [43] C. Xu, E. Bonetto, and A. Ahmad, "Dynapix slam: A pixel-based dynamic slam approach," *arXiv preprint arXiv:2309.09879*, 2023.
- [44] C. Kerl, J. Sturm, and D. Cremers, "Robust odometry estimation for rgb-d cameras," in *2013 IEEE international conference on robotics and automation*. IEEE, 2013, pp. 3748–3754.
- [45] X. Yu, R. Shen, K. Wu, and Z. Lin, "Robust visual slam in dynamic environment based on motion detection and segmentation," *Journal of Autonomous Vehicles and Systems*, 2024. [Online]. Available: <https://api.semanticscholar.org/CorpusID:270957414>
- [46] R. Scona, M. Jaimez, Y. R. Petillot, M. Fallon, and D. Cremers, "Staticfusion: Background reconstruction for dense rgb-d slam in dynamic environments," in *2018 IEEE international conference on robotics and automation (ICRA)*. IEEE, 2018, pp. 3849–3856.
- [47] B. Bescos, J. M. Fácil, J. Civera, and J. Neira, "DynaSLAM: Tracking, mapping, and inpainting in dynamic scenes," *IEEE Robotics and Automation Letters*, vol. 3, no. 4, pp. 4076–4083, 2018.
- [48] L.-C. Chen, G. Papandreou, F. Schroff, and H. Adam, "Rethinking atrous convolution for semantic image segmentation," *arXiv preprint arXiv:1706.05587*, 2017.
- [49] K. He, X. Zhang, S. Ren, and J. Sun, "Deep residual learning for image recognition," in *Proceedings of the IEEE conference on computer vision and pattern recognition*, 2016, pp. 770–778.
- [50] T.-Y. Lin, M. Maire, S. Belongie, J. Hays, P. Perona, D. Ramanan, P. Dollár, and C. L. Zitnick, "Microsoft coco: Common objects in context," in *Computer Vision—ECCV 2014: 13th European Conference, Zurich, Switzerland, September 6–12, 2014, Proceedings, Part V 13*. Springer, 2014, pp. 740–755.
- [51] J. Li, X. Pan, G. Huang, Z. Zhang, N. Wang, H. Bao, and G. Zhang, "Rd-vio: Robust visual-inertial odometry for mobile augmented reality in dynamic environments," *IEEE Transactions on Visualization and Computer Graphics*, 2024.
- [52] M. Tancik, V. Casser, X. Yan, S. Pradhan, B. Mildenhall, P. P. Srinivasan, J. T. Barron, and H. Kretschmar, "Block-nerf: Scalable large scene neural view synthesis," in *Proceedings of the IEEE/CVF Conference on Computer Vision and Pattern Recognition*, 2022, pp. 8248–8258.
- [53] S. Cortés, A. Solin, E. Rahtu, and J. Kannala, "Advio: An authentic dataset for visual-inertial odometry," in *Proceedings of the European Conference on Computer Vision (ECCV)*, 2018, pp. 419–434.